ORIGINAL PAPER

Ionoluminescence

physica status solidi a

www.pss-a.com

In Situ Characterization and Modification of β-Ga_2O_3 Flakes Using an Ion Micro-Probe

Marco Peres, Luis C. Alves, Flávia Rocha, Norberto Catarino, Carlos Cruz, Eduardo Alves, Ana G. Silva, Encarna G. Víllora, Kiyoshi Shimamura, and Katharina Lorenz*

In situ characterization of β-Ga_2O_3 flakes during proton irradiation is performed using ionoluminescence and electrical measurements. The quenching of the native blue-UV emission bands due to irradiation-induced defects in real time is monitored by ionoluminescence. Measurements of the *I–V* characteristics during irradiation present a good response of Ga_2O_3 for particle detection and a good radiation resistance.

1. Introduction

β-Ga_2O_3, with its wide band gap of 4.8 eV and high breakdown voltage, is a promising material for high power and high temperature electronics. Similar to mature semiconductor technologies, in particular silicon industry, ion implantation could greatly enhance the diversity of possible device designs allowing selective area doping and isolation as well as a control of dopant and defect profiles. The successful activation of implanted donor ions as well as optical dopants has already been demonstrated.[1–3] However, little is known about the processes leading to implantation damage build-up and its annealing.[4–6] Furthermore, understanding the interaction of radiation with this material is important to assess its potential for electronics used in radiation environment or even as a radiation detector.

The large breakdown voltage,[7] makes β-Ga_2O_3 an interesting material for particle detectors with a low leakage current and high charge collection efficiency. Recently it was demonstrated that metal-semiconductor-metal (MSM) photodetectors with one ohmic and one Schottky contact are interesting to develop radiation sensors because they can work in two different modes: in forward-bias mode exhibiting a high photosensitivity and in reverse-bias mode with a fast time response determined by the depletion region near the Schottky contact.[8] In this context, ion beam analysis (IBA) techniques with depth and lateral resolution and with the potential to modify the intrinsic properties by creating different types of defects, are especially suitable to study/optimize these electronic devices.[9] Irradiation studies complemented with real time measurements are particularly interesting for β-Ga_2O_3 devices since oxygen vacancies (donors) created by irradiation can be monitored optically and electrically by the related blue emission[10] and the decrease in electrical resistivity, respectively.

Many works have demonstrated the potential of ion beams as probes for materials characterization within a broad range of energies from keV to MeV.[9,11] When the ion beam crosses the material, different interactions occur between the energetic ions and the atoms of the target material. Different types of point and structural defects are produced by nuclear interactions. At high irradiation energies, electronic interactions lead to the ionization of the target atoms, i.e., creating a large number of electron–hole pairs in semiconductors.[12] At low and medium energies, defects are mainly created through nuclear interactions i.e., elastic collisions between the ions and the target nuclei which, depending on their recoil energies, can give rise to collision cascades. The profile of the continuous energy-loss along the ion path can be easily simulated using Monte Carlo-based programs, such as SRIM.[13] Particle-induced X-ray emission (PIXE) and Rutherford backscattering spectrometry (RBS) are two of the various well-established IBA techniques for materials characterization based on the nuclear and electronic interactions. Despite the high sensitivity of these techniques to the chemical composition they are almost insensitive to defects. In this context, complementary techniques like ion beam-induced luminescence (in the following called ionoluminescence, IL) and in situ electrical characterization can contribute to

Dr. M. Peres, Dr. K. Lorenz
IPFN, INESC-MN, Instituto Superior Técnico (IST), Campus Tecnológico e Nuclear
Estrada Nacional 10, P-2695-066 Bobadela LRS, Portugal
E-mail: marcoperes@ctn.tecnico.ulisboa.pt

Dr. L. C. Alves
C2TN, Instituto Superior Técnico (IST), Campus Tecnológico e Nuclear
Estrada Nacional 10, P-2695-066 Bobadela LRS, Portugal

F. Rocha, N. Catarino, C. Cruz, Dr. E. Alves
IPFN, Instituto Superior Técnico (IST), Campus Tecnológico e Nuclear
Estrada Nacional 10, P-2695-066 Bobadela LRS, Portugal

Prof. A. G. Silva
CEFITEC, Departamento de Física, Faculdade de Ciências e Tecnologia, Universidade Nova de Lisboa, Campus de Caparica
P-2829-516 Caparica, Portugal

Dr. E. G. Víllora, Dr. K. Shimamura
National Institute for Materials Science
1-1 Namiki, Tsukuba 305-0044, Japan

DOI: 10.1002/pssa.201800190

understanding the formation and behavior of specific defects.[14] Different types of point and structural defects are produced by nuclear interactions and intensive ionization. In this context, IL can be used directly to monitor the formation and quenching of optically active defects through the luminescence evolution during the irradiation with the ion beam.[15] In some cases, this can give information on the charge state or the local environment of a specific defect.[16] Beyond the optical properties, many works have demonstrated the potential of ion beams to modify the electrical properties by creating and/or passivating defects.

In this work, thin flakes of β-Ga_2O_3 were used to make MSM devices with lateral configuration, namely two lateral back-to-back Schottky diodes. The potential of these devices for radiation detectors was studied using an upgraded experimental IBA chamber which will be briefly described in the following.

2. Experimental Section

2.1. The μ-Probe Set-Up for In Situ Analysis

An upgrade was performed to the experimental chamber connected to the nuclear μ-probe installed at the 2.5 MV Van de Graaff accelerator at LATR (Laboratório de Aceleradores e Tecnologias de Radiação) at IST. Based on the Oxford Micro beams OM 150 quadrupole triplet system the LATR μ-probe allows the use of proton and He^+ beams with energies from ≈0.5 to 2.4 MeV and currents that can be controlled up to ≈10 nA using two sets of slits as described in more detail in ref. [17]. The beam can be routinely focused to ≈4 μm diameter and scanned over a sample area of 2.6 × 2.6 mm^2 for 2 MeV protons. For large irradiation areas the area can be defined by defocusing the punctual beam using the focusing lens. More details on the used microprobe end-station including the in-vacuum and the external beam setup can be found elsewhere.[15,16,18]

The referred experimental chamber upgrade was performed in order to allow in situ electrical characterization as well as ionoluminescence (IL) measurements simultaneously with conventional IBA techniques as PIXE and RBS. **Figure 1** shows a schematic of the chamber with the distribution of the different detectors associated with the different characterization techniques. The new modalities are integrated in the chamber lid and include a new sample holder allowing a gross vertical translation and horizontal tilt to align large samples and to control the incidence angle of the beam. The sample holder is attached to the cold finger of a closed-cycle liquid nitrogen cryostat for measurements from 77 K to room temperature. The fine horizontal and vertical alignment of the beam on the sample is performed through the magnetic quadrupole triplet of the beam scanning system.[12] The lid also contains the feedthroughs for the electrical signals using triaxial cables for low-noise measurements. The electrical measurements are performed with the help of an Agilent B1500 semiconductor device parameter analyzer. A home-made printed circuit board (PCB) was designed to connect the cables from the semiconductor analyzer to the sample.

This system allows a wide range of high precision *I–V* measurements, namely spot, sweep, and sampling (*I*/*V*-*t*) in continuous or pulsed mode. Ionoconductivity that consists in measuring variations of the conductivity induced by the ion beam is performed by synchronizing the *I–V* and *I*/*V*-*t* measurements with the ion beam irradiation.

In order to optimize the light collection in the IL set-up (described in ref. [19]), the previous mirror assembly was replaced by a focusable collimator system. The latter is composed of two fused silica lenses with 11 mm diameter mounted in a tube. The first lens with a focal length of 25 mm and a solid angle of 0.6 steradians collects and collimates the light while the second one focuses the light to the entrance of an optical fiber with a core diameter of 600 μm. The main advantage of this upgrade is the significant increase of the collection solid angle from ≈0.02 to ≈0.6 steradians. The light acquisition is performed using a monochromator working in the range of 200–900 nm and a high sensitivity and high speed CCD array (Jobin-Yvon Symphony) with a readout rate from 20 kHz to 1 MHz.

2.2. Device Preparation

β-Ga_2O_3 single crystals were grown by a floating zone (FZ) technique using two halogen lamps.[20] 4N Ga_2O_3 powder was shaped into a rod with a cold isostatic press and then sintered under air at 1450 °C for 10 h. A β-Ga_2O_3 single-crystal was used as seed, and the recrystallization was carried out under a constant N_2/O_2 gas flow rate of 0.25 L min^{-1}. The main impurity of the raw material was Si, which is well known to be an efficient donor. Therefore, the grown crystal had a typical carrier concentration and a conductivity in the order of ≈10^{18} cm^{-3} and ≈50 Ω^{-1} cm^{-1}, respectively. In order to obtain thin flakes of β-Ga_2O_3 the crystal was cut, cleaved, and at least mechanically exfoliated using a self-release tape (REVALPHA), as described in ref. [21]. These thin flakes were free from the commonly observed micro-twinning present in β-Ga_2O_3 crystals grown by the FZ, so that the full-width-at-half-maximum of the rocking curve is expected to be well below 100 arcsec. The flakes were transferred to a SiO_2/Si substrate with an isolating SiO_2 layer of 2 μm thickness. The two electrodes were formed by melting two squares of indium foil with dimensions of ≈1 × 1 mm and thickness of 0.5 mm with a separation of about 1 mm (see **Figure 2**a) and b)). Therefore, the performance of these devices depends on the properties of the two Schottky barriers formed at the metal/semiconductor interfaces and on the conductivity of the β-Ga_2O_3 flake between the two contacts. An equivalent circuit of this type of device is described by two back-to-back Schottky diodes connected by a resistance, as described in refs. [22,23]. Thus, independent of the signal of the applied voltage, one Schottky barrier is always reversely and the other one forwardly biased.

2.3. Irradiation Conditions

The optical and electrical characterizations using the ion micro probe were performed at room temperature. For the IL studies, an area of 500 × 200 μm^2 was irradiated using a similar flake as the one presented in Figure 2b) with a constant beam current of

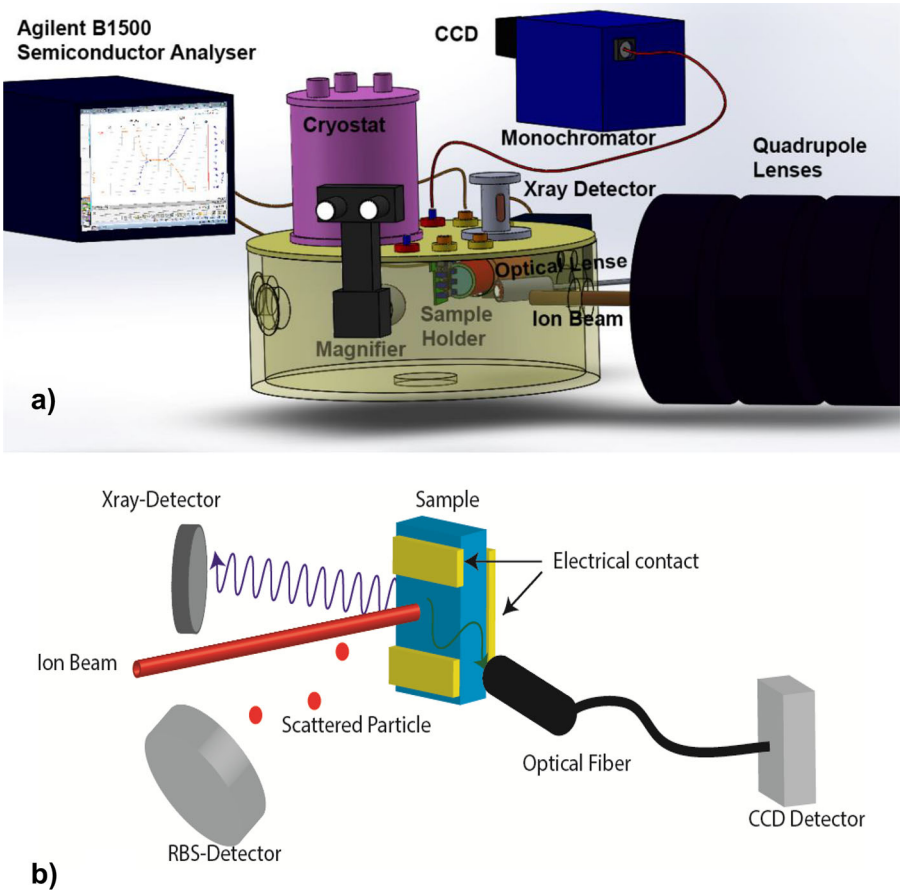

Figure 1. a) Schematic of the chamber coupled to the ion μ-probe. The beam is controlled by an electromagnetic quadrupole lens system. The feedthroughs for electrical and optical signals are located at the top of the chamber. The manually controlled sample holder allows the vertical displacement and the horizontal tilt of the sample holder. It is prepared to work with a cold finger to perform studies from room temperature down to 77 K using a liquid nitrogen cryostat. b) Schematic of the relative positions of the different collectors/detectors (PIXE, RBS, and ionoluminescence).

500 pA which corresponds to a constant flux of $\approx 3 \times 10^{12}$ protons/($cm^2\,s^{-1}$). For the electrical characterization (performed in the device presented in Figure 2b)), an area of $500 \times 500\,\mu m^2$ was irradiated between the two indium electrodes with a constant beam current of 500 pA corresponding to a flux of 1.25×10^{12} protons/($cm^2\,s^{-1}$).

3. Results and Discussion

Figure 3 shows the results of PIXE, RBS, and IL, all performed during irradiation with 2 MeV protons in a region between the two electrodes as well as an *I–V* curve (Figure 3d) which was acquired before the irradiation. The PIXE spectrum in Figure 3a) shows the presence of Ga together with a small Cr and Fe contamination. The spectrum deconvolution and quantitative analysis was performed with the GUPIXWIN software code,[24] giving for Cr and Fe the amounts of 55 ± 11 and $300 \pm 15\,\mu g\,g^{-1}$, respectively.

Figure 3b) shows the obtained RBS spectrum, where the barriers of Ga and O from β-Ga_2O_3 and the Si from the substrate, are clearly seen. The individual contributions of Ga, O, and Si fitted using the software DAN32[25] are also presented in the

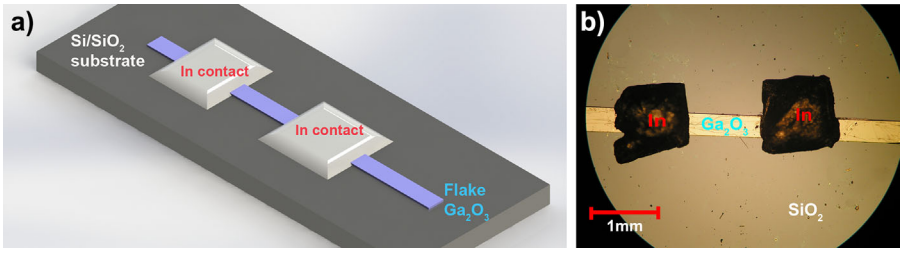

Figure 2. a) Schematic of the device with a metal-semiconductor-metal structure. b) Microscopy image of the device consisting of two indium contacts and a flake of Ga_2O_3.

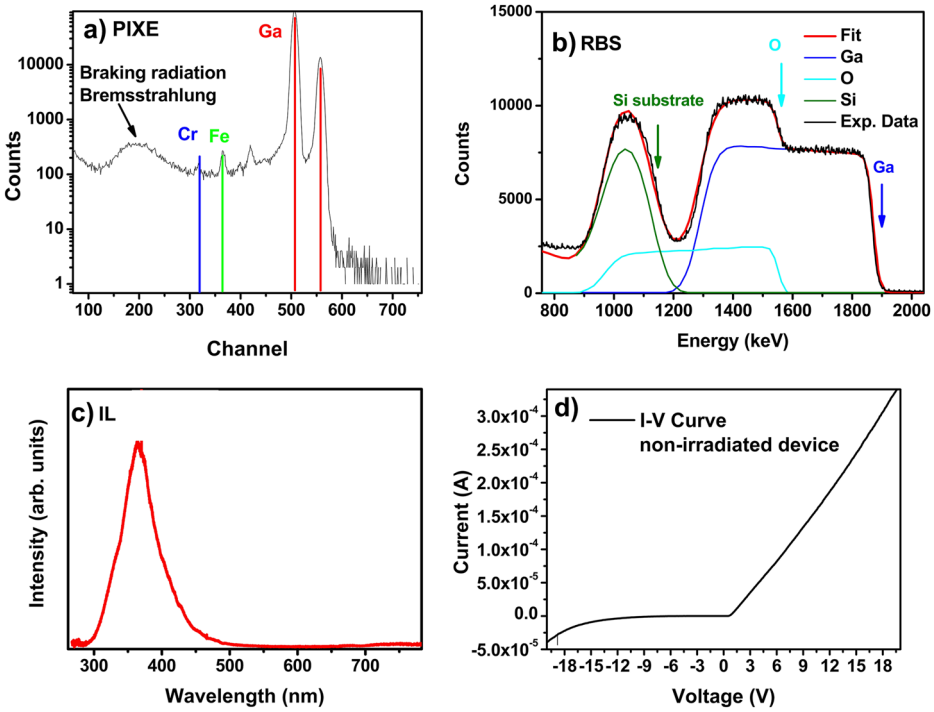

Figure 3. Experimental results acquired at room temperature on ≈5 μm thick β-Ga_2O_3 flake using the different characterization techniques: (a) PIXE, (b) RBS, (c) ionoluminescence, and (d) *I–V* sweep.

same figure. The fit of the RBS spectrum presented in the same figure (red line) is consistent with stoichiometric β-Ga_2O_3 and indicates that the thickness of the used flake is about 4.8 μm. For MeV protons the differential backscattering cross-section (especially for light elements) is no longer defined by the simple Rutherford cross-section. In particular for Si, a strong variation in the cross- section (resonance) can be observed at the incident proton energy of 1650 keV that leads to the observed Si contribution to the spectrum. The RBS signal acquired during each measurement is of particular importance since it allows determining the total charge used for each measurement and to correct/normalize the IL intensity when fluctuations in the beam current occur during the irradiation time. Figure 3c) shows the IL spectrum acquired during the first 20 s of irradiation. This spectrum is characterized by a broad band, spreading from the UV (300 nm) to the blue/green (500 nm) spectral region. This band is frequently attributed to an overlap of different recombination processes involving free electrons, self-trapped excitons, donor–acceptor pair recombination, and specific impurities.[26–29] The maximum of the emission is located in the UV at 367 nm (3.378 eV). According to Binet and Gourier,[26] this suggests that most of the emission in our samples are caused by the recombination of self-trapped excitons.[26,27]

The *I–V* curve of this device (Figure 3d)) is characterized by a non-linear and non-symmetric shape, confirming that the MSM device has non-ohmic contacts and that the two contacts have distinct Schottky barrier characteristics.[22]

Figure 4a) shows the evolution of the IL spectra of a similar Ga_2O_3 thin flake used to produce the devices based on Ga_2O_3 flakes, during an irradiation of about ≈1 h with a constant flux of ≈3×10^{12} protons/($cm^2\ s^{-1}$). The intensity of the luminescence decreases monotonously during the irradiation and no shape change nor energy shift occurs. Therefore, the defects created by irradiation are optically inactive, acting mainly as competitive, non-radiative recombination centers while the relative concentration of original optically active defects is not altered. Because no crystallinity changes were observed in previous studies of RBC/Channeling[6] (studies with a considerably higher irradiation fluence) performed in similar crystals to the ones used to obtain this thin

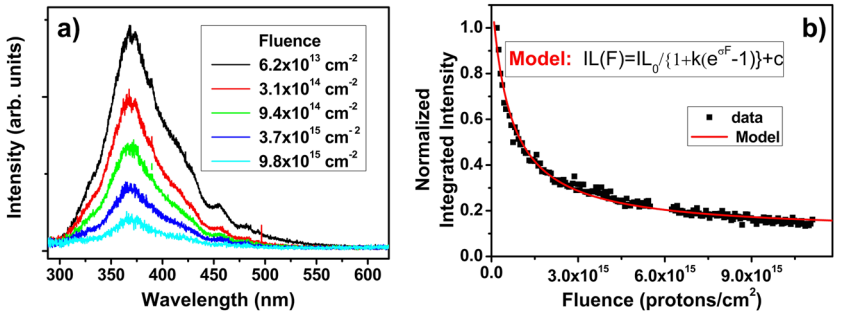

Figure 4. Ionoluminescence study at room temperature: (a) evolution of the ionoluminescence spectra with the fluence. b) Normalized integrated ionoluminescence intensity as a function of the fluence and fit using Equation (1).

Table 1. Parameters used for the fit shown in Figure 4b using Equation (1).

	IL_0	k	σ (cm^2)	Const
Fitted	1.05 ± 0.05	$(3.3 \pm 0.3) \times 10^4$	–	0.104 ± 0.008
Estimated by SRIM	–	–	4.72×10^{-20}	–

flake, the possible influence of crystallinity changes on the IL signal can be discarded. At last, the decrease of the IL intensity with the fluence is shown in Figure 4b). This decay is well fitted considering a model proposed by Sullivan and Baragiola[30] and described by the following equation:

$$IL(F) = \frac{IL_0}{1 + k(e^{\sigma F} - 1)} + const. \quad (1)$$

where IL_0 is the integrated intensity extrapolated to the time zero of the irradiation, F is the fluence, k and σ are two constants that describe the ratio of non-radiative to radiative transition rates and the effective cross section for damage of the radiative centers, respectively. In this work, in order to improve the quality of the fit, an extra constant term (*const.*) was considered. This constant describes the part of the IL that is independent of the irradiation fluence, possibly originating from an indirect process of excitation in a region far away from the one where primary nuclear or electronic interaction occurs (where most of the defects are created).[31] As pointed out by Santos et al.,[19] the parameters k and σ in Equation (1) influence each other making it difficult to determine their values accurately. Assuming that σ depends mostly on the defects created by displacements due to nuclear interaction, the σ value can be estimated by the average primary displacements produced per proton per unit length determined from SRIM simulations. Therefore, σ was given a value of $4.72 \times 10^{-20}\,cm^2$ from SRIM simulations by dividing the average primary displacements produced along the thickness of the flake ($\approx 5\,\mu m$), $5 \times 10^3\,cm^{-1}$ by the atomic density of β-Ga_2O_3 (1.06×10^{23} atoms cm^{-3} assuming a density of $4.95\,g\,cm^{-3}$). Assuming this value of σ, a value for k of 3.3×10^4 was obtained by fitting the luminescence quenching (Figure 4b) using Equation (1). Compared with diamond, with a k value of 310 estimated by the luminescence quenching of the donor–acceptor recombination localized at 433 nm,[30] the k value of β-Ga_2O_3 is significantly higher. Nevertheless, it is of the same order of magnitude as that reported by Santos et al.[19] for Mn-doped $ZnGa_2O_4$ fibres. This high k value suggests that the displacements promoted by the ion beam significantly increase the competitive non-radiative recombination channels relative to the radiative recombination ones. We cannot exclude a possible overestimation of k resulting from an underestimation of the σ value, by the fact that it was considered that σ only depends on the nuclear interaction and not on the dominant electronic interaction. **Table 1** summarizes the different fitting parameters extracted using Equation (1) and assuming the fixed σ estimated by SRIM.

To demonstrate the potential of the set-up to characterize and modify the electrical and electro-optical properties of a material/device, a study was performed irradiating the region between the contacts of a MSM device thus avoiding the depletion regions formed near the two metal contacts. Like this, an area of $500 \times 500\,\mu m^2$ was irradiated with 2 MeV protons with a constant flux of 1.25×10^{12} protons/($cm^2\,s^{-1}$), during 90 s resulting in a total fluence of $\approx 1 \times 10^{14}$ protons cm^{-2}.

Figure 5a) shows a series of *I–V* curves acquired in real time during the irradiation. A clear current gain is induced by the irradiation showing that the device acts as a radiation sensor. This proton-induced current is mainly resultant of an increment of the majority charge carrier concentration (i.e., electrons while holes have a very low mobility in β-Ga_2O_3) caused by additional free electrons excited by band-band and band-defect-band transitions.[32] The proton-induced current (which is defined by the difference between the *I–V* curves obtained with and without irradiation) varies almost linearly with the voltage, independently of the signal of the polarization (Figure 5b)). This is the kind of dependence expected for a current induced by extra free carriers generated by an external excitation.[33] The different slopes observed for positive and negative bias corroborate the different properties of the two non-ohmic contacts and are related with the differences in the Schottky barriers. Furthermore, no significant degradation of the *I–V* characteristics is seen up to the highest fluence of 1×10^{14} protons cm^{-2}. Considering the study of the luminescence quenching, an irradiation with 1×10^{14} protons cm^{-2} results in a luminescence reduction of about 14%. However, for a direct comparison of IL quenching (measured without applying any bias) and electrical properties another effect needs to be taken into account and studied in more detail in the future. Considering the low thermal conductivity of β-Ga_2O_3,[34] the influence of self-thermal-heating on the possible damage recovery during the *I–V* curves cannot be discarded.[35]

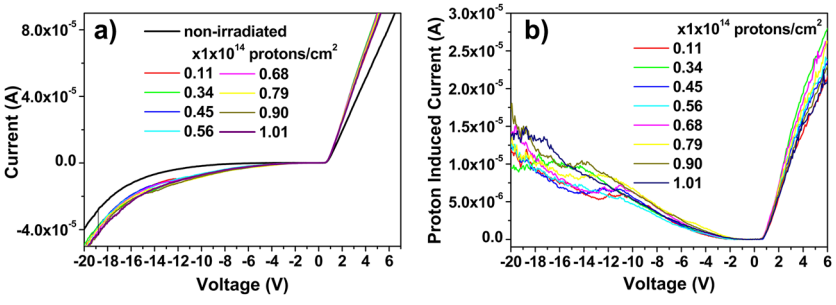

Figure 5. a) Multiple *I–V* sweeps during the irradiation. b) Proton-induced current (defined by the difference between the *I–V* curves obtained without and with irradiation).

The persistent proton-induced conductivity was studied performing transient measurements of the proton-induced current for the device biased with 5 V. **Figure 6**a) shows the evolution of the proton-induced current during and after three irradiation cycles of 150 s each with the same constant flux used to perform the *I–V* curves presented in Figure 5a). The three cycles of irradiation shown in Figure 6a) correspond to a total fluence of 5.6×10^{14} protons cm^{-2}. As can be seen in Figure 6a), the device reacts in a similar way to the proton beam for repeated

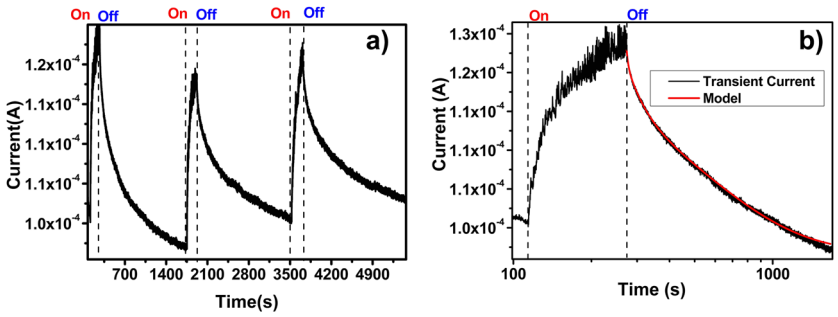

Figure 6. a) *I*/*V*-*t* transient measurements during three irradiation cycles of 150 s each. b) *I*/*V*-*t* transient measurement during the first irradiation cycle shown in (a); in this figure the fit (red line) using Equation (2) was included. These measurements were performed with the device biased at 5 V.

irradiation cycles, despite some fluctuations in gain and a slight increase of persistent current decay time attributed to defects created during the irradiation. Figure 6b) shows in more detail the rise of the current induced by the beam and the decay after switching off the beam for the first cycle. During the first 10 s a fast current increase is observed, which is then followed by a slowing increase rate that almost reaches saturation after 150 s. The fast proton-induced current increase is usually associated to band–band transitions, while the slow increase is often attributed to transitions involving deep defects and surface defects. After shutting off the beam (marked as "off" in Figure 6), a slow decay is observed (taking more than 20 min to decline to the intrinsic current). The decrease of the persistent proton-induced current (PPIC) with time is well fitted by three exponential decays according to the following equation:

$$I = I_{\text{intrinsic}} + I_1 e^{(-t/\tau_1)} + I_2 e^{(-t/\tau_2)} + I_3 e^{(-t/\tau_3)} \quad (2)$$

where $I_{\text{intrinsic}}$ is the intrinsic current (before irradiation) and I_1, I_2, I_3 are the three components of the proton-induced current with time decay constants τ_1, τ_2, and τ_3, respectively. **Table 2** summarizes the fitting parameters using this model. The three decays, with three different orders of magnitude, suggest that at least three different carrier recombination processes, are involved in the decay of the persistent conductivity. A recent work on photodetectors based on Ga_2O_3 suggested that the fast component with a decay time of 1.2 s is probably associated to band–band transitions.[32] However, Yamaga et al.[36] based on luminescence decay measurements suggest much faster decay times for the self-trapped exciton (in the microsecond range) and the authors attribute lifetimes longer than 1 s to distant electron–hole pairs with deep electron-trapped centers. Therefore, the slow components, in particular those with time constants of 46.9 and 469.5 s, may be associated with processes involving deep levels. In this context it is important to mention that Zhang et al.[37] have reported the presence of at least five deep levels related to different intrinsic defects of β-Ga_2O_3. Also, considering that the device is based on a thin flake produced by mechanical exfoliation, we cannot discard the role of surface defects and adsorption of molecules. In this context, it is noteworthy to mention that surface defects in β-Ga_2O_3 have been reported to lead to a band bending of up to 0.5 eV with a depletion width of several nanometers near the surface.[38] The surface band bending promoted by these defects can induce a spatial separation of the electron–hole pairs decreasing their recombination probability and resulting in a higher persistent current with a long decay time.[39] Indeed, surface defects can induce random potential fluctuations that can trap electrons and holes spatially separated in potential wells, resulting in a long recombination life time namely in band–band transitions.[40] Additionally, as in the case of other oxides like ZnO and MoO_3, strong persistent currents may also be associated with molecular desorption and adsorption at the surface, a dynamic process which can also induce a depletion region.[41–43]

4. Conclusions

The present study of proton irradiation and in situ characterization of a β-Ga_2O_3 MSM device demonstrates the potential of ion beams as probes for characterization and modification of materials. The capability to perform several measurements, such as optical, electrical, and compositional characterization, simultaneously and in real time allows studying the dynamics of defect formation and their effect on the physical properties of the material. IL spectra of our β-Ga_2O_3 samples are dominated by a broad emission band in the UV spectral region, typically attributed to the recombination of self-trapped excitons. Irradiation has a strong effect on the optical properties of β-Ga_2O_3, namely, inducing non-radiative recombination channels that quench the total emission without causing any change in the spectral shape. Nevertheless, the electrical characterization shows that the *I*–*V* characteristic is hardly affected by irradiation to the fluences studied in this work. A clear current gain during the irradiation of the device suggests its potential as a radiation sensor. However, the presence of persistent currents after switching off the proton beam, with a relaxation time in the order of several minutes, is an issue that needs to be understood and addressed for actual applications.

In order to elucidate the mechanism that determines the IL quenching and the electrical response of β-Ga_2O_3, additional IL studies with simultaneous electrical characterization will be

Table 2. Parameters used for the fit shown in Figure 6b using Equation (2) for the first irradiation cycle.

I_1 (A)	I_2 (A)	I_3 (A)	$I_{\text{intrinsic}}$ (A)	τ_1 (s)	τ_2 (s)	τ_3 (s)
$(1.8 \pm 0.1) \times 10^{-5}$	$(6.0 \pm 0.2) \times 10^{-6}$	$(1.9 \pm 0.2) \times 10^{-6}$	$(9.7 \pm 0.1) \times 10^{-5}$	470 ± 5	47 ± 2	4.1 ± 0.9

carried out in near future. In particular, the possible effect of self-heating, which can lead to damage recovery, needs to be investigated carefully.

Acknowledgments

This work was supported by the Fundação para a Ciência e a Tecnologia (FCT), Portugal grant PTDC/CTM-NAN/2156/2012. The authors express their gratitude to Filomena Baptista and Jorge Rocha for their availability and advice for the chamber design and optimization. M. Peres thanks FCT, Portugal for his post-doc grant, SFRH/BPD/111285/2015, K. Lorenz for the grant as Investigador FCT, and L.C. Alves for the FCT funding through the project UID/Multi/04349/2013.

Conflict of Interest

The authors declare no conflict of interest.

Keywords

β-Ga_2O_3, ionoluminescence, irradiation, micro-probe

Received: March 15, 2018
Revised: June 7, 2018
Published online: June 27, 2018

[1] K. Sasaki, M. Higashiwaki, A. Kuramata, T. Masui, S. Yamakoshi, *Appl. Phys. Express* **2013**, *6*, 086502.
[2] A. Gonzalo, E. Nogales, K. Lorenz, E. G. Víllora, K. Shimamura, J. Piqueras, B. Méndez, *J. Lumin.* **2017**, *191*, 56.
[3] E. Nogales, P. Hidalgo, K. Lorenz, B. Méndez, J. Piqueras, E. Alves, *Nanotechnology* **2011**, *22*, 285706.
[4] K. Lorenz, M. Peres, M. Felizardo, J. G. Correia, L. C. Alves, E. Alves, I. López, *Proc. SPIE* **2014**, *8987*, 89870M.
[5] E. Wendler, E. Treiber, J. Baldauf, S. Wolf, C. Ronning, *Nucl. Instrum. Methods Phys. Res. B* **2016**, *379*, 85.
[6] M. Peres, K. Lorenz, E. Alves, E. Nogales, B. Méndez, X. Biquard, B. Daudin, E. G. Víllora, K. Shimamura, *J. Phys. D. Appl. Phys.* **2017**, *50*, 325101.
[7] M. Higashiwaki, K. Sasaki, A. Kuramata, T. Masui, S. Yamakoshi, *Phys. Status Solidi Appl. Mater. Sci.* **2014**, *211*, 21.
[8] X. Sun, D. Li, Z. Li, H. Song, H. Jiang, Y. Chen, G. Miao, Z. Zhang, *Sci. Rep.* **2015**, *5*, 1.
[9] V. V. Kozlovskii, V. A. Kozlov, V. N. Lomasov, *Semiconductors* **2000**, *34*, 123.
[10] T. Onuma, S. Fujioka, T. Yamaguchi, M. Higashiwaki, K. Sasaki, T. Masui, T. Honda, *Appl. Phys. Lett.* **2013**, *103*, 041910.
[11] D. N. Jamieson, D. R. Beckman, A. A. Bettiol, J. S. Laird, K. K. Lee, S. Prawer, A. Saint, L. C. G. Witham, C. Yang, *Nucl. Instrum. Methods Phys. Res. B Beam Interact. Mater. Atoms* **1999**, *158*, 628.
[12] C. Udalagama, A. A. Bettiol, F. Watt, *Phys. Rev. B — Condens. Matter Mater. Phys.* **2009**, *80*, 224107.
[13] J. F. Ziegler, M. D. Ziegler, J. P. Biersack, *Nucl. Instrum. Methods Phys. Res. B* **2010**, *268*, 1818.
[14] P. D. Townsend, *Nucl. Instrum. Methods Phys. Res. B* **2012**, *286*, 35.
[15] C. Manfredotti, S. Calusi, A. Lo Giudice, L. Giuntini, M. Massi, P. Olivero, A. Re, *Diam. Relat. Mater.* **2010**, *19*, 854.
[16] J. Rodrigues, S. M. C. Miranda, M. Peres, E. Nogales, L. C. Alves, E. Alves, G. Tourbot, B. Daudin, B. Méndez, K. Lorenz, T. Monteiro, *Nucl. Instrum. Methods Phys. Res. B Beam Interact. Mater. Atoms* **2013**, *306*, 201.
[17] C. Alves, H. Breese, E. Alves, A. Paúl, M. R. da Silva, M. F. da Silva, J. C. Soares, *Nucl. Instrum. Methods Phys. Res. B Beam Interact. Mater. Atoms* **2000**, *161–163*, 334.
[18] V. Corregidor, A. R. Oliveira, P. A. Rodrigues, L. C. Alves, *Nucl. Instrum. Methods Phys. Res. B Beam Interact. Mater. Atoms* **2015**, *348*, 291.
[19] N. F. Santos, A. J. S. Fernandes, L. C. Alves, N. A. Sobolev, E. Alves, K. Lorenz, F. M. Costa, T. Monteiro, *Nucl. Instrum. Methods Phys. Res. B Beam Interact. Mater. Atoms* **2013**, *306*, 195.
[20] E. G. Villora, K. Shimamura, Y. Yoshikawa, K. Aoki, N. Ichinose, *J. Cryst. Growth* **2004**, *270*, 420.
[21] R. Mitdank, S. Dusari, C. Bülow, M. Albrecht, Z. Galazka, S. F. Fischer, *Phys. Status Solidi* **2014**, *211*, 543.
[22] Z. Zhang, K. Yao, Y. Liu, C. Jin, X. Liang, Q. Chen, L. M. Peng, *Adv. Funct. Mater.* **2007**, *17*, 2478.
[23] A. J. Chiquito, C. A. Amorim, O. M. Berengue, L. S. Araujo, E. P. Bernardo, E. R. Leite, *J. Phys. Condens. Matter* **2012**, *24*, 225303.
[24] J. L. Campbell, N. I. Boyd, N. Grassi, P. Bonnick, J. A. Maxwell, *Nucl. Instrum. Methods Phys. Res. B Beam Interact. Mater. Atoms* **2010**, *268*, 3356.
[25] G. W. Grime, *Nucl. Instrum. Methods Phys. Res. B Beam Interact. Mater. Atoms* **1996**, *109*, 170.
[26] L. Binet, D. Gourier, *J. Phys. Chem. Solids* **1998**, *59*, 1241.
[27] E. G. Víllora, T. Atou, T. Sekiguchi, T. Sugawara, M. Kikuchi, T. Fukuda, *Solid State Commun.* **2001**, *120*, 455.
[28] T. Harwig, F. Kellendonk, S. Slappendel, *J. Phys. Chem. Solids* **1978**, *39*, 675.
[29] T. Onuma, S. Fujioka, T. Yamaguchi, M. Higashiwaki, K. Sasaki, T. Masui, T. Honda, *Appl. Phys. Lett.* **2013**, *103*, 041910.
[30] P. A. Sullivan, R. A. Baragiola, *J. Appl. Phys.* **1994**, *76*, 4847.
[31] A. V. Krasheninnikov, K. Nordlund, *J. Appl. Phys.* **2010**, *107*, 071301.
[32] S. Oh, Y. Jung, M. A. Mastro, J. K. Hite, C. R. Eddy, J. Kim, *Opt. Express* **2015**, *23*, 28300.
[33] T. S. Moss, *Rep. Prog. Phys.* **1965**, *28*, 15.
[34] E. G. Víllora, K. Shimamura, T. Ujiie, K. Aoki, *Appl. Phys. Lett.* **2008**, *92*, 202118.
[35] M. H. Wong, Y. Morikawa, K. Sasaki, A. Kuramata, S. Yamakoshi, M. Higashiwaki, *Cit. Appl. Phys. Lett.* **1935**, *1091*, 123511.
[36] M. Yamaga, T. Kishita, E. G. Villora, K. Shimamura, *Opt. Mater. Express* **2016**, *6*, 3135.
[37] Z. Zhang, E. Farzana, A. R. Arehart, S. A. Ringel, *Appl. Phys. Lett.* **2016**, *108*, 052105.
[38] T. C. Lovejoy, R. Chen, X. Zheng, E. G. Villora, K. Shimamura, H. Yoshikawa, Y. Yamashita, S. Ueda, K. Kobayashi, S. T. Dunham, F. S. Ohuchi, M. a. Olmstead, *Appl. Phys. Lett.* **2012**, *100*, 181602.
[39] R. Calarco, M. Marso, T. Richter, A. I. Aykanat, R. Meijers, A. V. D. Hart, T. Stoica, H. Luth, *Nano Lett.* **2005**, *5*, 981.
[40] Y.-C. Wu, C.-H. Liu, S.-Y. Chen, F.-Y. Shih, P.-H. Ho, C.-W. Chen, C.-T. Liang, W.-H. Wang, *Sci. Rep.* **2015**, *5*, 11472.
[41] Q. H. Li, T. Gao, Y. G. Wang, T. H. Wang, *Appl. Phys. Lett.* **2005**, *86*, 123117.
[42] D. R. Pereira, M. Peres, L. C. Alves, J. G. Correia, C. Díaz-Guerra, A. G. Silva, E. Alves, K. Lorenz, *Surf. Coat. Technol.* **2018**, https://doi.org/10.1016/j.surfcoat.2018.01.034, in press.
[43] A. Johannes, R. Niepelt, M. Gnauck, C. Ronning, *Appl. Phys. Lett.* **2011**, *99*, 252105.